




## Article

# Sensitivity Analysis of the Catalysis Recombination Mechanism on Nanoscale Silica Surfaces

Lichao He <sup>1</sup>, Zhiliang Cui <sup>1</sup>, Xiangchun Sun <sup>1</sup>, Jin Zhao <sup>1,2,3,\*</sup>  and Dongsheng Wen <sup>1,4,\*</sup>

<sup>1</sup> School of Aeronautical Science and Engineering, Beihang University, Beijing 100191, China; zanjiaochaoshu@buaa.edu.cn (L.H.); by1805107@buaa.edu.cn (Z.C.); sunxch1979@buaa.edu.cn (X.S.)

<sup>2</sup> Ningbo Institute of Technology, Beihang University, Ningbo 315100, China

<sup>3</sup> Hangzhou Innovation Institute (Yuhang), Beihang University, Hangzhou 310052, China

<sup>4</sup> Lehrstuhl für Thermodynamik, Technical University of Munich, 80333 Munich, Germany

\* Correspondence: jin.zhao@buaa.edu.cn (J.Z.); d.wen@buaa.edu.cn (D.W.)

**Abstract:** A deep understanding of surface catalysis recombination characteristics is significant for accurately predicting the aeroheating between hypersonic non-equilibrium flow and thermal protection materials, while a de-coupling sensitivity analysis of various influential factors is still lacking. A gas–solid interface (GSI) model with a hyperthermal flux boundary was established to investigate the surface catalysis recombination mechanisms on nanoscale silica surfaces. Using the reactive molecular dynamics (RMD) simulation method, the effects of solid surface temperature, gas incident angle, and translational energy on the silica surface catalysis recombination were qualified under hyperthermal atomic oxygen (AO), atomic nitrogen (AN), and various AN/AO gas mixtures' influence. It can be found that, though the Eley–Rideal (E–R) recombination mechanism plays a dominant role over the Langmuir–Hinshelwood (L–H) mechanism for all the sensitivity analyses, a non-linear increasing pattern of AO recombination coefficient  $\gamma_{O_2}$  with the increase in incident angle  $\theta_{in}$  and translational energy  $E_k$  is observed. Compared with the surface catalysis under hyperthermal AO impact, the AN surface adsorption fraction shows an inverse trend with the increase in surface temperature, which suggests the potential inadequacy of the traditional proportional relationship assumptions between the surface adsorption concentration and the surface catalysis recombination coefficient for other species' impact instead of AOs. For the incoming bi-component AO/AN gas mixtures, the corresponding surface catalysis coefficient is not the simple superposition of the effects of individual gases but is affected by both the intramolecular bond energies (e.g., O<sub>2</sub>, N<sub>2</sub>) and intermolecular energies (e.g., Si/N, Si/O).

**Keywords:** surface catalysis recombination; silica surface; reactive molecular dynamics; sensitivity analysis; thermal protection material



**Citation:** He, L.; Cui, Z.; Sun, X.; Zhao, J.; Wen, D. Sensitivity Analysis of the Catalysis Recombination Mechanism on Nanoscale Silica Surfaces. *Nanomaterials* **2022**, *12*, 2370. <https://doi.org/10.3390/nano12142370>

Academic Editor: Gregory M. Odegard

Received: 9 June 2022

Accepted: 5 July 2022

Published: 11 July 2022

**Publisher's Note:** MDPI stays neutral with regard to jurisdictional claims in published maps and institutional affiliations.



**Copyright:** © 2022 by the authors. Licensee MDPI, Basel, Switzerland. This article is an open access article distributed under the terms and conditions of the Creative Commons Attribution (CC BY) license (<https://creativecommons.org/licenses/by/4.0/>).

## 1. Introduction

As the flying speed increases, the extreme aeroheating brings the problem of the “heat barrier”, which is the major barrier for the next generations of high-speed aircraft [1,2]. An in-depth understanding of how aerothermal heat is generated and how to accurately predict the amount of heat produced is of paramount importance for designing reliable thermal protection systems (TPS) [3–5].

The high-temperature thermo-chemical non-equilibrium gas flows due to the high speed, i.e., Mach number > 5, cause extremely complicated heterogeneous interactions, such as surface catalysis, oxidation, and ablation, between the gas and TPS materials [6–8]. Silica is an important material that has been widely used in non-ablative TPS [9,10], which has the characteristics of thermostability, anti-ablative, and shock resistance [11]. Due to the high-temperature gas effect, the surrounding air may become dissociated into atomic form, i.e., atomic oxygen and nitrogen, whose interactions with the silica surface display remarkable differences from that of molecular impact [12]. For air at 1 atm pressure, oxygen

dissociation begins at about 2000 K and is completed at about 4000 K. At that temperature, nitrogen dissociation begins, and  $N_2$  is essentially totally dissociated at about 9000 K. The air, originally considered to be composed of 79%  $N_2$  and 21%  $O_2$ , can therefore be assumed as a five-species model ( $N_2$ ,  $O_2$ , NO, N and O). The recombination of dissociated atomic oxygen (AO) or atomic nitrogen (AN) due to the high temperature's effect on their gaseous compounds on the silica surface is a typical surface catalytic exothermic reaction, which significantly affects the prediction of aeroheating [6,13]. For instance, a weak catalytic surface could cause a large decrement in surface heat flux as it prevents the recombination of the dissociated atoms on the surface, hence reducing exothermic heat releases. The determination of the catalytic effect, termed as "recombination coefficient", becomes crucial [14–16].

Traditional numerical strategies such as Computational Fluid Dynamics (CFD) modeling always employ a constant catalytic coefficient assumption to predict the aerodynamic heating, termed non-catalytic (i.e.,  $\gamma = 0$ ), fully-catalytic (i.e.,  $\gamma = 1$ ), or a finite catalytic assumption [17], which results in a large difference in the estimation of heat flux. It has been shown that the predicted aerodynamic heat could differ 3–4 times [17,18] in the stagnation point under hypersonic reentry flow conditions by using either a non-catalytic or fully-catalytic assumption. Aiming to accurately predict aerodynamic heating, scholars have developed the finite catalytic model [18–20]. However, the catalytic recombination coefficient in the finite catalytic model comes from the fitting of the experimental results; the results of different experiments are significantly varied [21–23], leading to different simulation results. For instance, the oxygen prepared by Dicken et al. [24] contained a small amount of water molecules, and the  $-OH$  ions produced by the ionization of water molecules bonded to the surface sites of the test piece, resulting in the reduction in the surface catalytic recombination coefficient. Stewart et al. [25,26] used emission spectrum atomic diagnosis to obtain atomic concentration, which was based on the assumption that all tracer atoms had made a transition, hence a large discrepancy in the measurement of atomic concentration. Carleton et al. [27] obtained the catalytic recombination coefficient by measuring the atomic O loss, rather than the reaction products. Consequently, other products such as  $O_3$  may interfere with the accuracy of the catalytic recombination coefficient, leading to a much higher measured catalytic recombination coefficient. Balat et al. [23] conducted the experiments at 200 Pa, but the experimental method was difficult to eliminate the error caused by the  $O_2$  molecules formed in the gas phase. Considering the large uncertainties among different techniques, it becomes extremely difficult to unify a reliable recombination coefficient from different experimental results, as shown in Figure 1. From a microscopic simulation front, Rutigliano et al. [28] only calculated the E–R reaction mechanism via DFT investigation, so the data they obtained are lower and the trend is different from other conclusions. Consequently, the thermal protection system (TPS) needs to use high design margins to protect the inner structure due to the uncertainty of the recombination coefficient and the lack of mechanistic understanding [17], especially the microscopic phenomena at the gas–solid interface [29]. In this regard, molecular dynamics simulation can provide a promising solution to advance the catalytic reaction mechanism at the microscale [30–32].

Recently, an atomistic-scale numerical technique using Reactive Force Field (ReaxFF) potential based on a classical Molecular Dynamics (MD) simulation method, also known as the Reactive Molecular Dynamics (RMD) method, has been proposed to reveal more microscopic features that contribute to the more accurate determination of the catalytic effects [33–35]. Quite a few RMD studies have been conducted to investigate the heterogeneous reactions between atomic oxygen impact onto typical TPS materials such as graphene, silica, and different metallic surfaces [36–38]. Cui et al. [39,40] studied the effects of the incident angle of AO, energy flux density, the number of graphene layers, and the surface morphology on the ablation, and found that the surface morphology had a significant effect on the ablation rate. Bačová et al. [41] presented an investigation of dynamics relations in thick films of cis-polybutadiene chains placed between rough amorphous silica slabs.

The results suggested that the monomeric translational motion parallel to the surface was affected by the presence of the silica slab. Gai et al. [42] established the Pt/O/H reaction force field and derived the theoretical adsorption isotherms of O and H on the Pt slab and nanoparticles by using a GCMC/RMD mixed simulation. Jeon et al. [43] simulated the oxidation process of copper on different surfaces and showed that the initial oxidation was determined by the surface energy via analyzing the growth process of copper oxide and the change of surface morphology. Valentini et al. [44] simulated the adsorption process of O<sub>2</sub> impacting the Pt slab and observed that the adsorption probability of O<sub>2</sub> increased with the incident energy in the range of 0.1–0.4 eV of O<sub>2</sub> incident energy. Chen et al. [45] simulated the early oxidation process of the Si(100) surface and illustrated that oxygen transport was the dominant factor in the initial oxidation process. The formation of the oxide layer would subsequently hinder oxygen transport and prevent further oxidation, and the increase in temperature could promote the migration of oxygen to the deep Si layer. Cao et al. [46] changed the surface dimer density of Si by biaxial tensile strain and revealed that the dimer plays an important role in the surface oxidation reaction by modifying the adsorption amount and penetration depth of O. Newsome et al. [47] established a ReaxFF reaction force field of Si–Si, Si–O, and Si–H, and showed that SiC gradually transformed into silicon oxide and formed graphite-like layers. In the presence of excess O<sub>2</sub>, the graphite-like layer was further oxidized to CO and CO<sub>2</sub>. Gamalo et al. [48] simulated the collision of CO on the surface of preoxygenated  $\beta$ -cristobalite(001), including molecular reflection and non-dissociative molecular adsorption. CO<sub>2</sub> was formed in a small range by the Eley–Rideal reaction. Mao et al. [49] studied the reaction process of CO on the surface of  $\beta$ -SiO<sub>2</sub> by using RMD and showed that the reaction of CO on the surface of  $\beta$ -SiO<sub>2</sub> was mainly molecular reflection and non-dissociation adsorption. With the increase in incident energy, the molecular reflection ratio increased, which verified the low reactivity of CO on the surface of  $\beta$ -SiO<sub>2</sub>. Khalilov et al. [50–52] studied the growth mechanism of SiO<sub>2</sub> via atomic and molecular oxygen impacting Si and SiO<sub>2</sub> surfaces. It was found that the thickness of the oxide layer only depended on the incident energy when the temperature was below 700 K, but became reliant on both incident energy and surface temperature at temperatures over 700 K, due to the increased penetration and diffusion rate of the oxidant at higher temperatures. Yang et al. [53] simulated the reaction process of the O atom and  $\beta$ -SiO<sub>2</sub> surface at different temperatures under the thermal equilibrium of wall and gas at 10 atm. It was found that the catalytic recombination coefficient obtained by RMD was in good agreement with the experimental ones at high temperatures, but was higher at low temperatures.

To calculate the recombination coefficient, a gas–solid model is generally established. Previously, Cozmuta et al. [54] established a gas–solid model for the reaction of O<sub>2</sub> and N<sub>2</sub> mixed gases on an SiO<sub>2</sub> surface and revealed that the adsorption of the O atom on the SiO<sub>2</sub> surface was stronger than that of the AN atom. The gas column model can calculate the catalytic recombination coefficient, which, however, brought some statistical errors to the products due to the difficulty in ruling out the influence of the interactions among atoms/molecules in the gas phase. For instance, the reflected atoms may become recombined into molecules in the gas phase, which rendered some uncertainties in calculating the catalytic effect. Based on the gas column model of Cozmuta, Norman et al. [55–58] established a flux boundary model to study the catalytic recombination mechanism and site number of O atoms at different temperatures and pressures on the surface of  $\beta$ -SiO<sub>2</sub>. Such a flux boundary model eliminated the interference of gas reactions in the gas phase and increased the statistical accuracy catalytic recombination coefficient. This makes it possible to further analyze the influence of environmental factors such as temperature and pressure on the catalytic reaction.

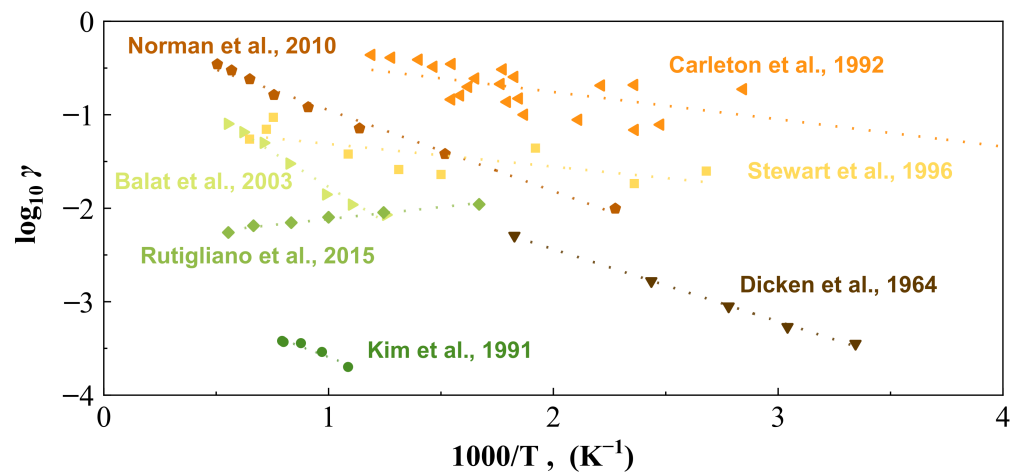


Figure 1. Typical silica surface catalysis recombination coefficient measurement values [23–28,55].

Such a brief review shows that our current understanding of the impact of hyperenthalpy atoms on TPS materials is still poor. Mostly single atom impact has been investigated under idealistic conditions based on a gas–solid column model. However, in a real flight, the surrounding gas is a mixture of N and O atoms or their molecule forms, and their contents also vary with different attack angles and flight heights due to different viscous heating effects. Many questions, such as the effects of different gas mixtures, the impact angle, and the impacting energies on the catalytic recombination over TPS materials, especially  $\text{SiO}_2$ , remain unanswered. We have recently established a gas–solid interface flux (GSI) model in RMD and successfully revealed the effects of solid surface morphology and impacting gas mixture on graphene and SiC surfaces [39,40], as well as the competing effects between surface oxidation and catalysis [59]. To answer the questions raised above, we will use the established flux boundary model to study the impact of different O/N mixtures under various conditions, including the effects of O / N atoms, incident angle, and incident translational energy, on  $\text{SiO}_2$  surfaces, and reveal their influences on the surface catalytic recombination, an area is of importance for the future design of silicon-based TPS materials.

## 2. Materials and Methods

All RMD simulations in the present work were carried out based on an open-source simulation software LAMMPS (Large-scale Atomic/Molecular Massively Parallel Simulator) [60] developed by Sandia National Laboratories. The  $\text{ReaxFF}_{\text{SiO}}^{\text{GSI}}$  force field, developed by Kulkarni et al. [61] was applied in the present work and had also been successfully employed to describe the chemistry and dynamics in oxygen–silica gas–surface interactions (GSI) [53,54,56].

A novel modified GSI model was established and extended based on the previous RMD research [54,55] with a modified flux boundary, as shown in Figure 2. Both gas and solid phases were modeled: (a) For the silica substrate (a typical non-ablative TPS material) as the solid phase, an  $\alpha\text{-SiO}_2$  plate cleavage along the (001) surface with a thickness of  $12 \text{ \AA}$  was prepared with a planar dimension of  $45 \times 45 \text{ \AA}^2$  in the  $x$ - and  $y$ -axis directions, respectively. To prevent the surface from moving downwards during the continuous gas collisions, the last layer of all the atoms for the silica slab was fixed. Moreover, apart from the atoms in the surface top-two atom layers, all the remaining atoms for the silica slab were heated and equilibrated with the Langevin thermostat [62], ensuring the temperature stability of the silica surface temperature during the bombardment of the impinging gas. (b) For the gas phase in this modified GSI model, a single oxygen or nitrogen atom was generated every 1.0 ps from a random horizontal position at a height of  $15 \text{ \AA}$  above the surface with a prescribed translational energy  $E_{\text{tr}}$  and incident angle  $\theta_{\text{in}}$ . The pressure at the micro/nano-scale gas–solid interface inside the boundary layer is very low during the



hypersonic flow conditions, which can be assumed as a one-by-one atom bombardment process for simulations to decouple the complicated thermal/mechanical/chemical interactions. It should be noticed that for the traditional GSI model, the  $z$  dimension of the simulation box was designed as long as 240 Å to prevent further recombination in the gas phase after collisions at the gas–solid interface [39]. However, the possible interactions and recombination as gas–gas reactions within this long gas column may lead to potential uncertainties or errors in properly identifying and evaluating the gas–surface interactions. To tackle this issue, a novel GSI model was modified with a flux boundary for the impinging gas, where all the species located 15 Å above the silica surface were analyzed every 1000 fs and then deleted to avoid further gas–gas interactions within the long gas column.

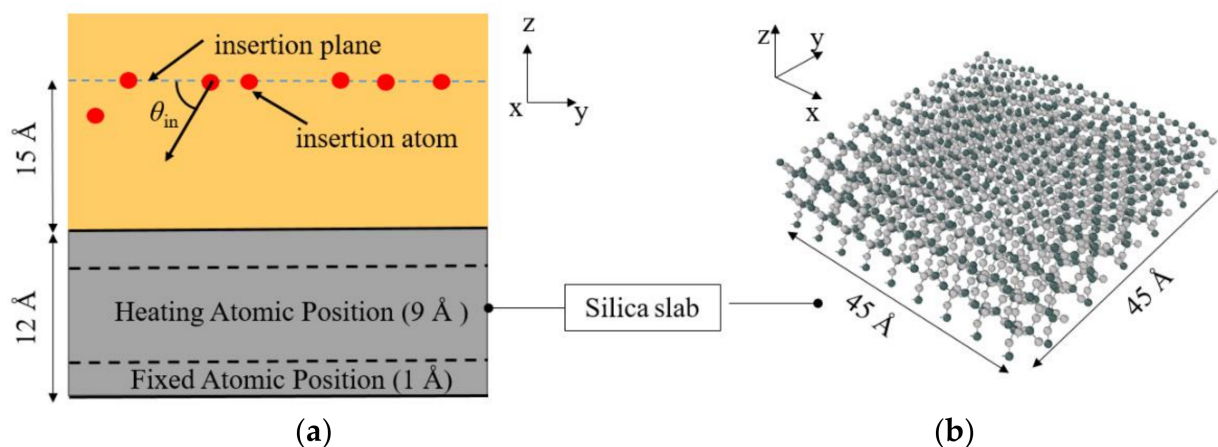


**Figure 2.** Schematic illustration of gas–solid interaction (GSI) model with flux boundary. (a) the RMD simulation configuration for the gas–solid interface (b) the silica surface configuration.

The silica surfaces for all the simulations were relaxed for 50 ps using the Nose/Hoover thermostat to achieve thermal equilibrium towards the target temperature with a time step of 0.25 fs before inserting any gaseous species onto the solid slab, then followed by simulation with a period of 1000 ps (To run a 1000-ps simulation took about 60 h with 16 processors). Reflective and periodical boundary conditions were employed in the directions parallel and perpendicular to the surface, respectively. To identify the surface temperature  $T_s$ , gas incident angle  $\theta_{in}$ , translational energy  $E_k$ , and mixture fraction effects on the silica surface catalysis recombination performance under both hyperthermal AO and AN flux bombardment, 38 models were analyzed in this work, whose detail parameters are shown in Table 1.

Since the material surface catalysis recombination coefficient is considered one of the most significant parameters, the evaluation results of the present work are calculated using the following formula:

$$\gamma = \frac{\text{Flux of atoms recombining at the surface}}{\text{Flux of atoms impinging on the surface}} \quad (1)$$

which is defined as the ratio of the impinging atoms that recombine at the surface over the total impinging atoms on the surface. It is notable that the Eley–Rideal (E–R) and Langmuir–Hinshelwood (L–H) recombination mechanisms are the two dominant mechanisms in the surface catalysis recombination process [63]. The E–R recombination mechanism refers to the recombination process in which the incoming oxygen atom, when hitting an adsorbed atom onto the surface, recombines into a molecule and then desorbs from the surface. In the L–H recombination mechanism, the molecule formation is caused by surface diffusion, enabling two atoms adsorbed on the surface to encounter each other for recombination. In order to better describe the surface catalytic effect, according to Deutschman’s research, the main surface reactions of AN/AO mixture gas are listed in Table 2. The symbol “(s)” denotes a free surface site and species with a label “(s)” are adsorbed at the surface. An analysis

code was further developed in this work to provide a detailed E–R and L–H recombination mechanism distinction through tracking the molecular oxygen generation pathways.

**Table 1.** Parameters of GSI models investigated in the present work.

Type	Model	Surface Temperature, $T_s$	Incident Angle, $\theta_{in}$	Incident Translational Energy, $E_k$	Incident Components, $f_{O/mixture}$
Benchmarking Case	1 (Standard)	1000 K	90°	0.05 eV	100%—full AO
Set I: Effect of silica surface temperature $T_s$	2–4	500 K, 1500 K, and 2000 K	90°	0.05 eV	100%—full AO
Set II: Effect of AO incident angle $\theta_{in}$	5–9	1000 K	15°, 30°, 45°, 60°, and 75°	0.05 eV	100%—full AO
Set III: Effect of AO incident translational energy $E_k$	10–16	1000 K	90°	0.01, 0.10, 0.50, 1.00, 2.00, 3.00, and 4.00 eV	100%—full AO
Set IV: Effect of $T_s$ , $\theta_{in}$ , and $E_k$ on silica surface catalysis performance with AN bombardment	17–20	500 K, 1000 K, 1500 K, and 2000 K	90°	0.05 eV	full AN
	21–26	1000 K	15°, 30°, 45°, 60°, 75°, and 90°	0.05 eV	full AN
	27–34	1000 K	90°	0.01, 0.05, 0.10, 0.50, 1.00, 2.00, 3.00, and 4.00 eV	full AN
Set V: Bicomponent monatomic gas mixture effect	35–38	1000 K	90°	0.05 eV	75% (AO: 75%; AN: 25%), 50% (AO: 50%; AN: 50%), 25% (AO: 25%; AN: 75%) and 0% (AO: 0%; AN: 100%)

**Table 2.** Surface reaction mechanisms.

Reaction	Mechanism
$O + (s) \rightarrow O(s)$	Adsorption
$N + (s) \rightarrow N(s)$	
$O(s) \rightarrow O + (s)$	
$N(s) \rightarrow N + (s)$	
$O_2(s) \rightarrow O_2 + (s)$	Desorption
$N_2(s) \rightarrow N_2 + (s)$	
$NO(s) \rightarrow NO + (s)$	
$O + O(s) \rightarrow O_2 + (s)$	E–R mechanism
$N + N(s) \rightarrow N_2 + (s)$	
$N + O(s) \rightarrow NO + (s)$	
$O + N(s) \rightarrow NO + (s)$	
$O(s) + O(s) \rightarrow O_2 + (s)$	L–H mechanism
$N(s) + N(s) \rightarrow N_2 + (s)$	
$N(s) + O(s) \rightarrow NO + (s)$	

### 3. Results and Discussion

#### 3.1. Validation and Temperature-Dependent Silica Surface Catalysis Characteristics

To demonstrate the validity of the applied ReaxFF<sub>SiO</sub><sup>GSI</sup> force field and calculation setup for the RMD simulations, the benchmark cases of the silica surface catalysis characteristics with variations of surface temperature are established and compared with both the reported

experimental and simulation results [23,24,26,55] in this section. Under the same AO gaseous phase incident conditions with a translational energy of 0.05 eV normal to the silica slab, four GSI models with flux boundaries are built up under four silica surface temperatures  $T_s$ , i.e., 500 K, 1000 K, 1500 K, and 2000 K, respectively.

Both the transient flow-field analysis during the AO continuous bombardment and material response analysis are identified as shown in Figure 3. It can be observed that except for the slight amount of  $O_3$  molecules, the molecular oxygen  $O_2$  dominates the compositions of all the gaseous products. It also demonstrates that the heterogeneous surface catalysis recombination reaction is playing the leading role during the gas–surface interactions [ $O + O \rightarrow O_2$ ]. Moreover, with the increase in silica surface temperature  $T_s$ , the molecular oxygen  $O_2$  generation rate becomes larger. This can be explained by a detailed material response analysis for the silica slabs with an insight into the AO surface adsorption conditions, as shown in Figure 3b,c. There is no big change in the amount of  $O_3$  molecule generation due to the fact that the  $O_3$  molecule has longer and weaker bonds than the  $O_2$  molecule. Therefore, it only appears as the intermediate product, which has high energy barriers as an unstable product in a negligible amount. Figure 3b shows that for all the simulation cases, the adsorption rate of monatomic oxygen atoms on the surface of the  $SiO_2$  slab is quite high at the early stage to around 300 ps, followed by smoothing out the distinguishing spike due to the saturation of the active sites for the silica surface. Moreover, a larger surface coverage fraction of oxygen adsorption is found for the silica surface model with higher equilibrium temperature, which can also be visualized as presented in Figure 3c, implies the higher possibilities of surface catalysis recombination reactions with both L–H and E–R recombination mechanism pathways.

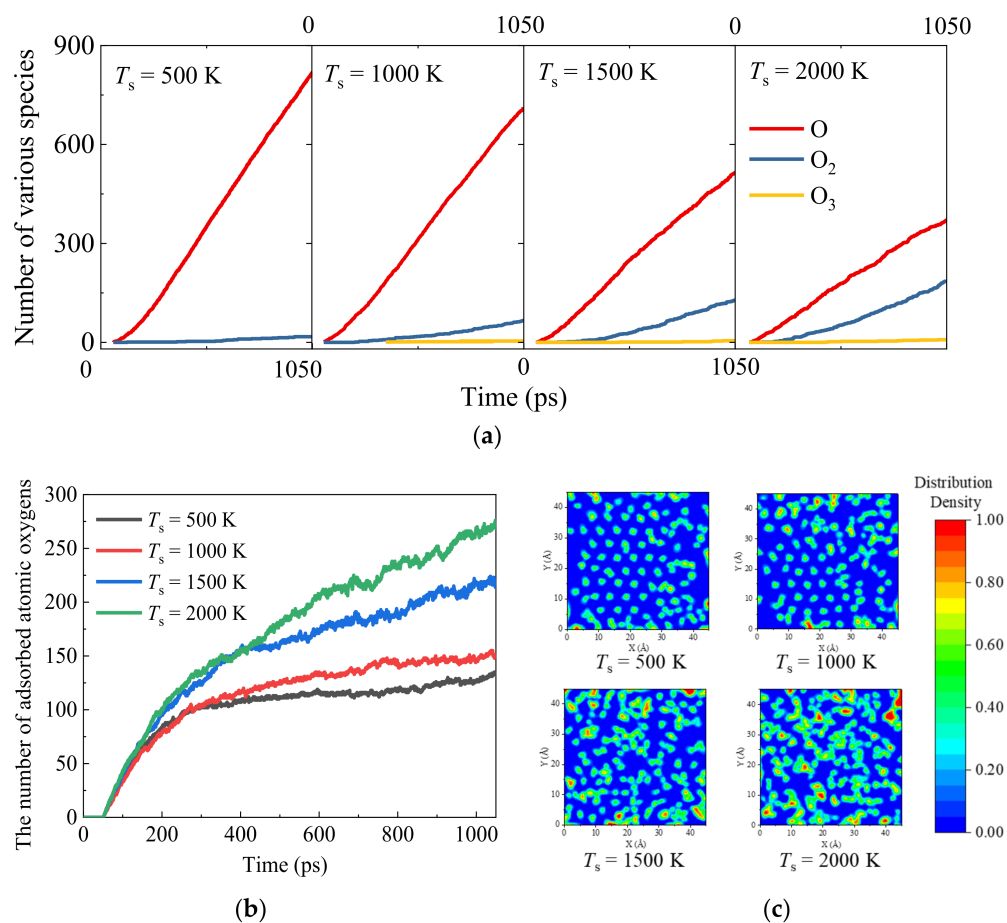


**Figure 3.** Surface adsorption of oxygen atoms for Models 1–4. (a) The number of various species in the gaseous phase, (b) the number of oxygen atoms adsorbed with variations of time, and (c) the effects of silica surface temperature on the saturated oxygen-atom density distribution.

As shown in Figure 4a, the silica surface temperature-dependent recombination coefficients obtained by RMD simulation results show an exponential trend, which is comparable to the RMD results obtained by Norman et al. [55]. The activation energy of the surface catalysis reactions is further obtained by the linear fitting of the logarithm of the catalytic recombination coefficient with variations of the reverse of surface temperature, as shown in Figure 4b. The quantified activation energy from RMD simulations is compared with both reported experimental and simulation values, as presented in Table 3. It can be found that the activation energy value for surface catalysis reactions obtained by RMD simulation methods is slightly lower than those from experimental measurements. This can be explained by the fact that for RMD simulations, the silica surface is cleaved along the (001) plane, leaving a large number of high-energy suspended Si atoms on the skin layer. Meanwhile, under the experimental conditions, the Si atoms can be oxidized rapidly or form a Si-OH bond with water as it is exposed to air, leading to a reduction in the surface catalytic recombination coefficient value of the SiO<sub>2</sub> surface.

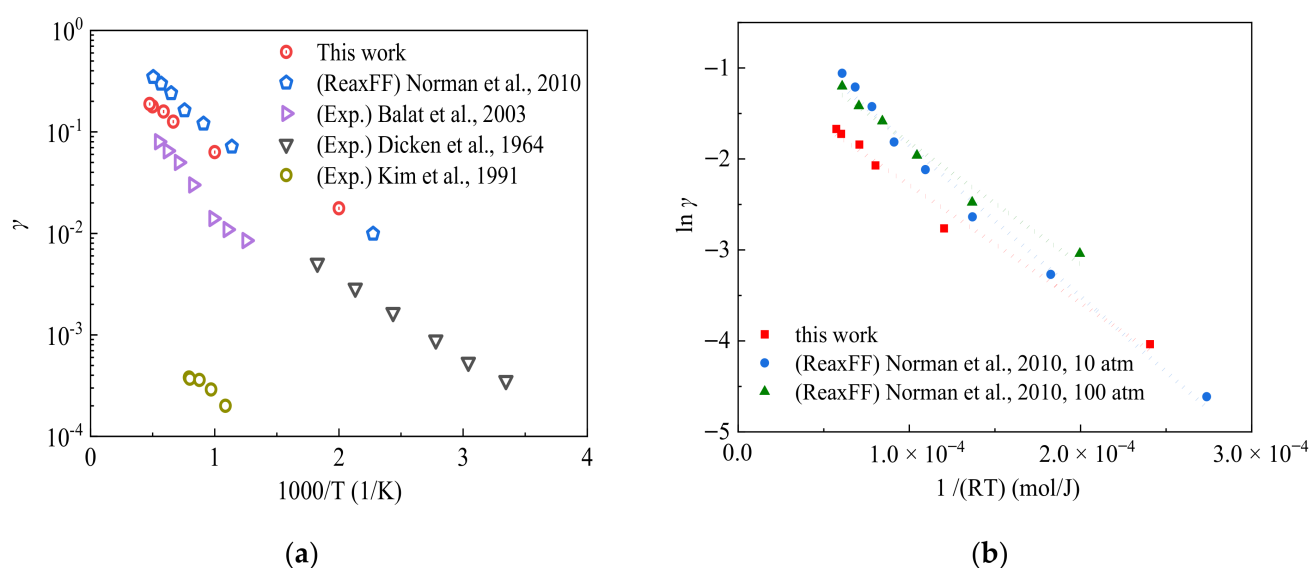


**Figure 4.** Comparisons of calculated surface catalytic recombination coefficient and the activation energy by Models 1–4. (a) The calculated surface catalysis recombination coefficient [23,24,26,55], and (b) the calculated activation energy [55].

**Table 3.** Comparison of the activation energy for surface catalysis reactions of Models 1–4.

Source	Activation Energy
This work	$0.134 \pm 0.008$ eV
Norman et al. [55]	$0.138\text{--}0.172 \pm 0.012$ eV
Balat et al. [23]	$0.296 \pm 0.019$ eV
Dicken et al. [24]	$0.153 \pm 0.040$ eV
Kim and Bourdard [26]	$0.166 \pm 0.020$ eV

To identify the molecular oxygen generation pathways due to the surface catalysis characteristics, further efforts are made to provide a detailed E–R and L–H recombination mechanism distinction using an own-developed code with its working flow chart, as shown in Figure 5. The transient trajectories of all atomic oxygens recombined with the molecular oxygens are captured at the gas–solid heterogeneous interface (within a height of 1.5 Å from the silica surface [54]). The E–R surface catalysis recombination mechanism is classified if monatomic oxygen collides with another oxygen atom adsorbed onto the silica surface by tracing oxygen history trajectories, otherwise, the L–H mechanism is considered.

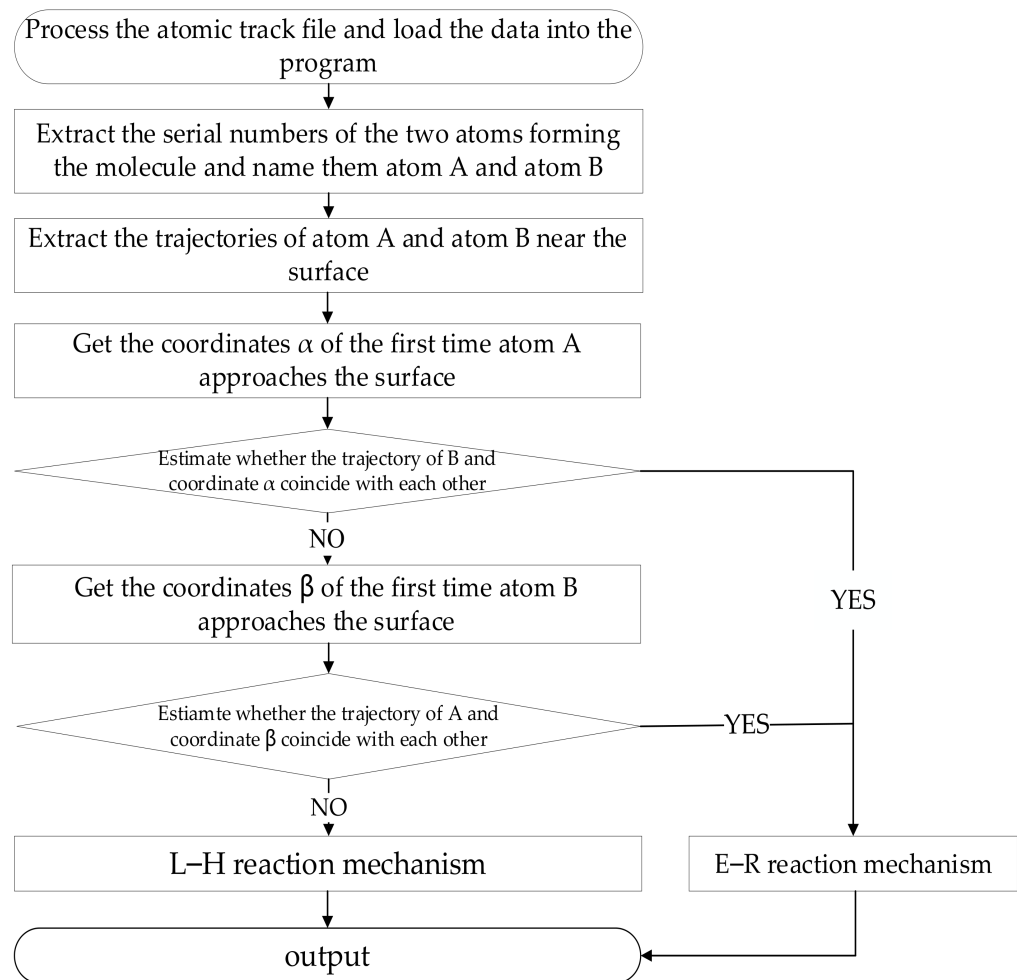


**Figure 5.** Statistical flow chart of surface catalysis recombination mechanism analysis.

The chemical reaction pathways of the surface catalysis phenomenon can be clearly visualized, as shown in Figure 6a, with an easy identification of the classic E–R and L–H recombination mechanisms. (a) The adsorption process: the adsorption behavior of the impinging oxygen atoms happens at the early stage, forming  $\equiv\text{Si}-\text{O}\bullet$  sites onto the silica surfaces. (b) The recombination process: colliding with another incoming high-enthalpy oxygen atom, an  $\equiv\text{Si}-\text{O}_2$  group is formed from the original  $\equiv\text{Si}-\text{O}\bullet$  site which is known as a key feature in the E–R recombination mechanism. In addition, the recombination due to the diffusion between two adjacent  $\equiv\text{Si}-\text{O}\bullet$  sites may also lead to the reformation of the  $\equiv\text{Si}-\text{O}_2$  group, which is known as the L–H recombination mechanism. The similar diffusion L–H recombination behavior is also visualized between  $\equiv\text{Si}-\text{O}\bullet$  and  $\equiv\text{Si}-\text{O}_2$  groups, reforming an  $\equiv\text{Si}-\text{O}_3-\text{Si}\equiv$  group as an intermediate. (c) The desorption process: the chemical bonds in the functional groups between the Si and O atoms break and the  $\text{O}_2$  molecule is generated and released from the silica surface.

Through identifying the molecular oxygen gas generation pathways, the E–R surface catalysis recombination mechanism is found to account for the dominant proportions during the continuous bombardment of monatomic oxygens under various temperature conditions, as shown in Figure 6b. The  $\text{O}_2$  molecule formation originated from the E–R recombination mechanism is measured as high as 83% for the surface temperature  $T_s$  equilibrated at 500 K. With the increase in the silica surface temperature  $T_s$  to 2000 K, the surface coverage fraction of AO becomes greater due to the larger number of active sites on the silica surface at elevated temperature, enhancing the percentages of L–H recombination reactions with diffusion recombination mechanisms for molecular oxygen formations.



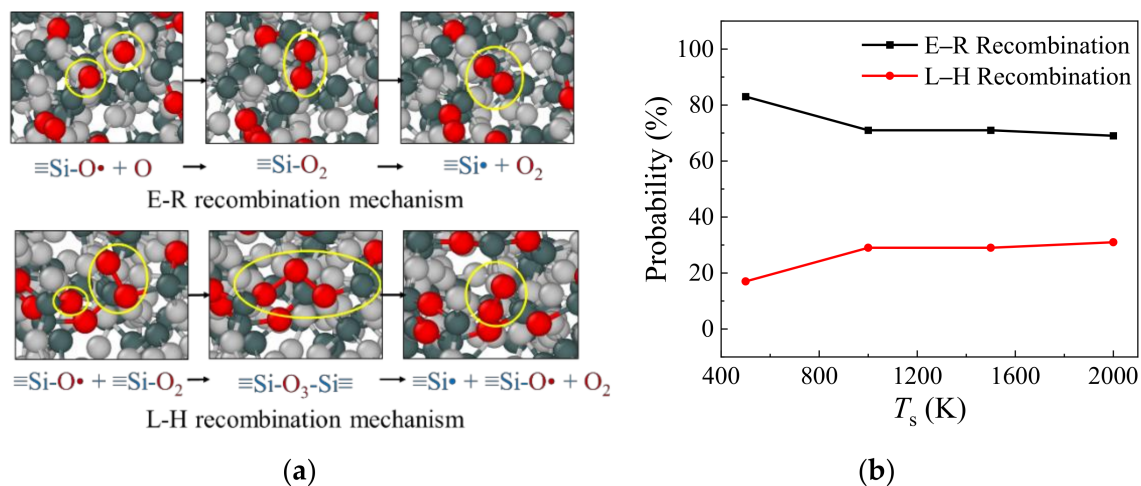


**Figure 6.** Surface catalysis recombination mechanism analysis by Models 1–4. (a) Illustration snapshots for the E–R and L–H recombination mechanisms, and (b) the effect of surface temperature on the surface catalysis recombination mechanisms.

### 3.2. Effects of AO Incident Angle and Translational Energy

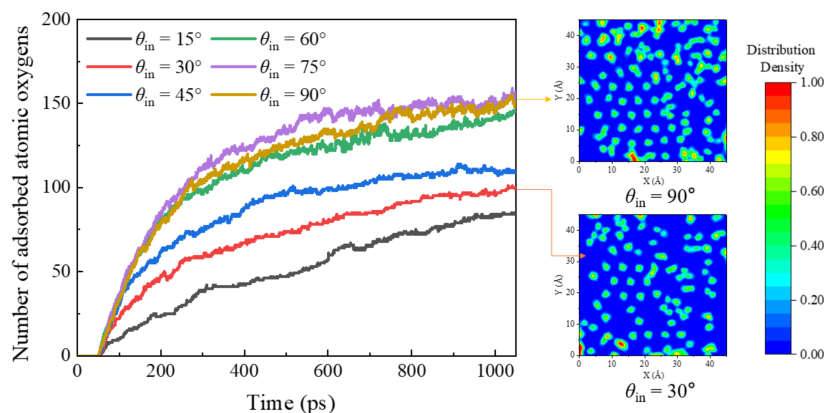
Considering that the incident AO angle is not always perpendicular to the surface and the incident energy also varies with the speed, six sets of RMD calculations are carried out to investigate the AO incident angle effect on the silica surface catalysis characteristic in a range of angles of attack from  $15^\circ$  to  $90^\circ$  under different translational energy impact.

#### 3.2.1. The Effect of AO Incident Angle

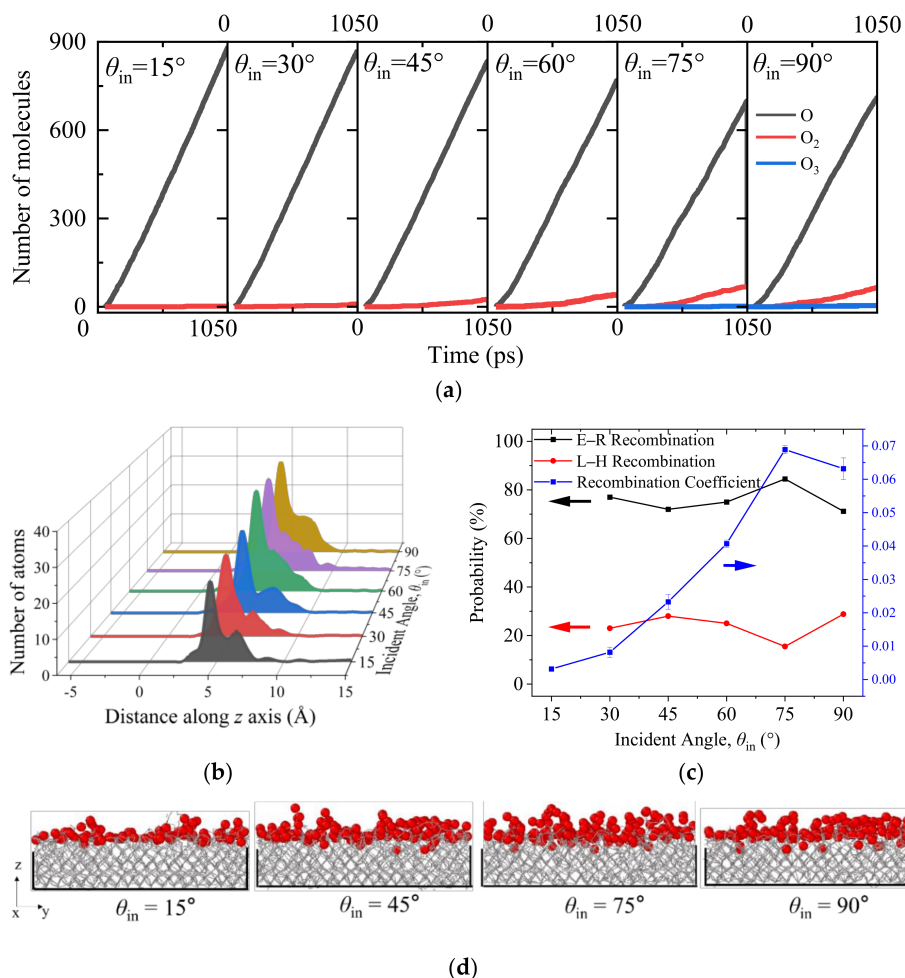
Figure 7 demonstrates the effect of monatomic AO incident angle on the surface adsorption situation with snapshot illustrations of the saturated silicon-dioxide surface. It indicates that the first step of heterogeneous recombination involves the probability of AO adsorption during a gas-phase collision at a clean surface site, where AO acts as the oxidizer. Transient surface adsorption profiles with various AO incident angles imply that the AO adsorption rate is quite large at the early stage, followed by a flattening out due to the saturation of adsorption on active sites of the silica surface. Moreover, this adsorption process is found to be not only temperature-dependent but also incident-angle-dependent, with a comparative observation that with a high angle of incidence, i.e.,  $\theta_{\text{in}} = 90^\circ$ , the surface coverage fraction of AOs is significantly larger than that with a small angle of incidence, i.e.,  $\theta_{\text{in}} = 30^\circ$ .

Figure 8 further quantifies the AO incident angle effect on the gas flow field, silica material response, and the surface catalysis recombination characteristics, and three observations are found. (I) Generally speaking, with the increase in incident angle  $\theta_{\text{in}}$ , the generated  $\text{O}_2$  molecules increase due to the surface catalysis effect, while at the same time, more AO atoms in the flow field are consumed, so the number of AOs is reduced, as shown in Figure 8a. Taking the incident angle  $\theta_{\text{in}}$  of  $15^\circ$  as an illustration, due to its small vertical velocity component perpendicular toward the silica surface, both the fraction of collisions that have sufficient energy to react and the fraction of sufficiently energetic collisions that actually react for adsorption, recombination, and desorption are reduced. Therefore, though carrying the same incoming translational energy, it is more difficult for AOs with a smaller incident angle  $\theta_{\text{in}}$  to complete the surface catalysis recombination reaction. (II) The surface catalysis recombination coefficient  $\gamma$  is sensitive to the incident angle in a non-linear increasing trend with the increase in AO incident angle  $\theta_{\text{in}}$ , as shown in Figure 8c. (III) A peak value  $\gamma$  of 0.068 is observed to occur when the incident angle  $\theta_{\text{in}}$  is around  $75^\circ$  (rather than  $90^\circ$ ), which is consistent with the lowest final saturation state of z-density profiles of AOs adsorbing at the silica interface, as shown in Figure 8b, where it indicates the highest adsorption rate for AOs occurring at  $\theta_{\text{in}} \sim 75^\circ$ . This observation

shows a good agreement with the results from Norman et al. [58] and suggests that there is an optimal relationship between the incident angle and translational energy to achieve the highest surface catalytic recombination rate.



**Figure 7.** The effect of AO incident angle on the surface adsorption situation with snapshot illustrations of the saturated silicon dioxide surface by Models 1 and II-5-9.



**Figure 8.** The effect of oxygen incident angle on the flow field, material response, and the silica surface catalysis characteristics by Models 1 and II-5-9. (a) The statistics of various species in the gaseous phase during the collisions, (b) the incident angle effect on the saturated z-density profiles of oxygen atoms on the silica surface, (c) the calculation of surface catalysis recombination coefficient and the detailed recombination mechanism analysis, and (d) snapshots for the final AO surface adsorption status.

### 3.2.2. The Effect of Incoming AO Translational Energy

To further identify the effect of incoming AO translational energy on the surface catalysis recombination characteristics, eight models of incoming AO bombardment with various AO incidence translational energy  $E_k$ , i.e., from 0.01 to 4.00 eV, are established with a constant surface temperature  $T_s$  of 1000 K.

The transient surface adsorption profiles for the silica slab under the impact of AOs with various incident translational energy are presented in Figure 9. It can be similarly observed that the AOs initially adhere at the activation sites on the surface, followed by the silica surface adsorption gradually reaching its saturation state. Combining with the final saturated silica surface adsorption contours captured at the gas–solid interface, the AO adsorption saturation state on the silica surface with larger incident translational energy  $E_k$  (e.g., 1.00 eV) is much denser than that with smaller  $E_k$  (e.g., 0.05 eV). This is due to the fact that the increase in AO incident translational energy may provide sufficient energy for the adsorption and oxidation reactions after surface collisions. In addition, it can be found that the surface adsorption saturation state becomes independent of the incident translational energy in the range of 1.00–4.00 eV.

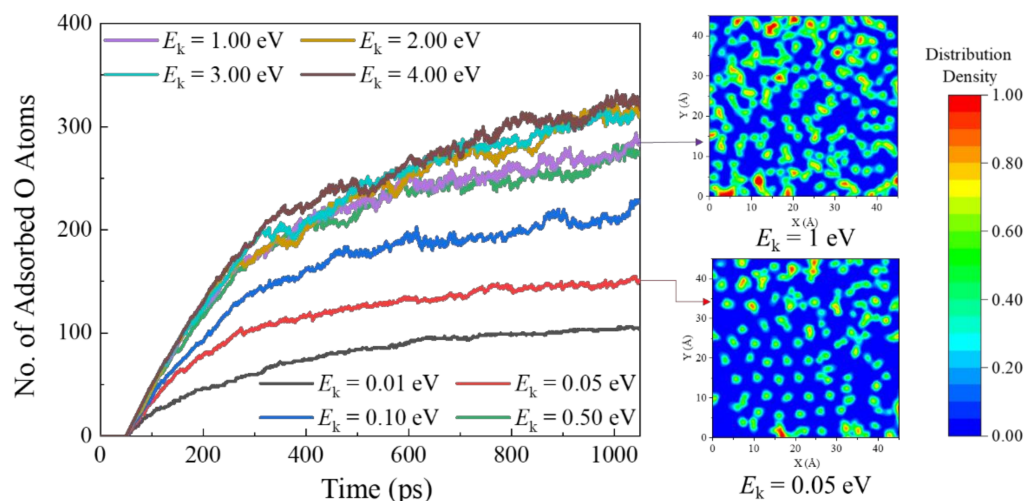


**Figure 9.** The effect of monatomic oxygen incident translational energy on the surface adsorption situation with snapshot illustrations of the saturated silicon dioxide surface by Models 1 and III-10-16.

The effect of AO incident translational energy on the flow field, material response, and the silica surface catalysis characteristics is analyzed in Figure 10. Through tracking the flow field component during the AO continuous impact as presented in Figure 10a, the number of molecular oxygens increases with the increase in AO incident translational energy due to the surface catalysis recombination reactions; correspondingly, the number of AOs in the flow field decreases. It should be noted that when the incident translational energy is greater than 1.00 eV, small quantities of  $O_3$  molecules are observed. The denser surface adsorption saturation and deeper surface erosion state for the silica slab under the impact of AO carrying larger incident kinetic energy can be visualized in the  $z$ -density profiles as shown in Figure 10b. The impact of AOs carrying higher kinetic energy may cause some incident oxygen atoms to break through the silicon–oxygen bonds in the silica surface layer and embedding in-depth into the silicon dioxide plate, eroding the silica and damaging the internal structure of the silica surface, as visualized in Figure 10d.

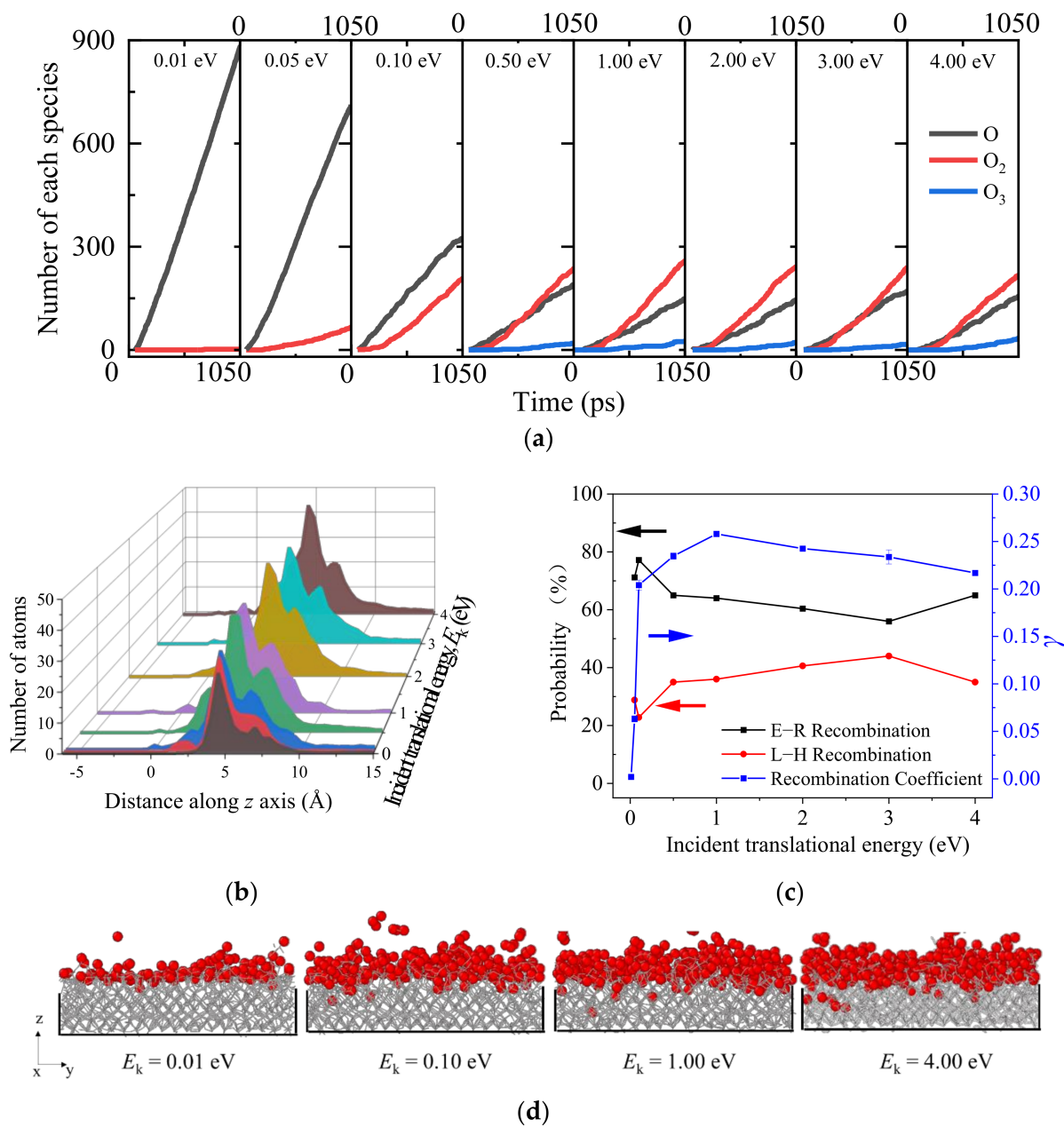


**Figure 10.** The effect of AO incident translational energy on the flow field, material response, and the silica surface catalysis characteristics by Models 1 and III-10-16. (a) The statistics of various species in the gaseous phase during the collisions, (b) the incident angle effect on the saturated z-density profiles of oxygen atoms on the silica surface, (c) the calculation of surface catalysis recombination coefficient and the detailed recombination mechanism analysis, and (d) snapshots for the final AO surface adsorption status.

As a result, the silica surface catalysis recombination coefficient variation as a function of AO incident translational energy is shown in Figure 10c. A continuous growth of  $\gamma$  from 0.002 to its peak value of 0.258 is obtained when the AO incident translational energy increases from 0.01 eV to 1.00 eV. A slight decline in  $\gamma$  is noticed when  $E_k$  is further increased from 1.00 eV to 4.00 eV, where the same E-R surface catalytic recombination shows as the dominant mechanism during the formation process of O<sub>2</sub> molecules. This can be explained by two reasons: (1) the incident AOs with high  $E_k$  greater than 1.00 eV tend to embed onto the silica surface due to too-high kinetic energy and directly bounce away from the surface without participating in the recombination reactions. (2) The small amount of

unstable reaction-product  $O_3$  molecules tend to be generated when there are incident AOs carrying kinetic energy greater than 0.50 eV, which leads to the competing effect for free AOs to further form  $O_2$  molecules, resulting in a slight reduction in the  $\gamma$  value with the increase in incidence translational energy greater than 1.00 eV.

### 3.3. The AN Gas Effect on the Silica Surface Catalysis

It has been recognized that under the high-enthalpy (>8.5 MJ/kg) aerodynamic environment, reactions occur in the shock layer and molecular oxygen is almost fully dissociated at the shock. The atomic oxygen is slightly below the equilibrium value because some oxygen is incorporated into NO. The relative amount of N, O, NO,  $N_2$ , and  $O_2$  at the gas–solid interface, therefore, varies on a case-by-case basis. To separate the behavior of N and O recombination on the silica surface at high temperature, a GSI model with a flux boundary for AN colliding with the  $SiO_2$  surface is established in this session, and the effects of silica surface temperature, incident angle, and incident translational energy on the surface catalysis recombination phenomenon are investigated in-depth in this session.

It has been identified that the surface catalysis recombination characteristics are closely dependent on the surface adsorption behaviors during the vertical impact of incoming dissociated gas [55]. Therefore, with an incident angle of  $90^\circ$  and an incident translational energy of 0.05 eV as the benchmark values, the effects of silica surface temperature on the transient surface adsorption status for the AN incidence as the gas phase toward the silica surface are analyzed in Figure 11. Compared with the AO impact, as shown in Figure 3, the AN surface adsorption fraction shows an inverse trend with the increase in surface temperature. The atomistic scale reason implies its close revelations with the bond energy difference among various species, where the intramolecular bond energy for  $N_2$  gas molecules ( $\sim 942$  kJ/mol) is much higher than the Si–N bond energy ( $\sim 355$  kJ/mol). Therefore, more adsorbed nitrogen atoms would be removed with the increase in the generated  $N_2$  gas molecules at higher surface temperatures. Conversely, the sparser AN surface adsorption may inversely restrain the surface catalysis recombination property. This extraordinary phenomenon suggests the potential inadequacy of the traditional proportional relationship assumptions [55] between the surface adsorption concentration and the surface catalysis recombination coefficient, as shown in Figure 11a, especially for species other than AO (where the bond energy impact is drowned out for AO incidence cases because the intramolecular bond energy for  $O_2$  gas molecules ( $\sim 497$  kJ/mol) is very close to the Si–O bond energy ( $\sim 452$  kJ/mol)).

In addition, the effects of AN incident angle and incident kinetic energy on the transient surface adsorption situations are analyzed in Figure 12. Combined with the calculated surface catalysis recombination coefficient, as shown in Figure 13a, a similar sensitivity response can be found compared with AO incidence scenarios. (I) A non-linear trend of  $\gamma$  is revealed for both incident angle  $\theta_{in}$  and incident kinetic energy  $E_k$  effects. (II) A larger influential magnitude of  $E_k$  is observed for AN surface catalysis performance compared with the  $\theta_{in}$  impact. The corresponding AN recombination mechanism for all the investigated sensitive factors is quantified at the nanoscale and shown in Figure 13b by comparisons with that of AO. A similar E–R recombination type is found to be dominant for AN bombardment toward the silica material surface.



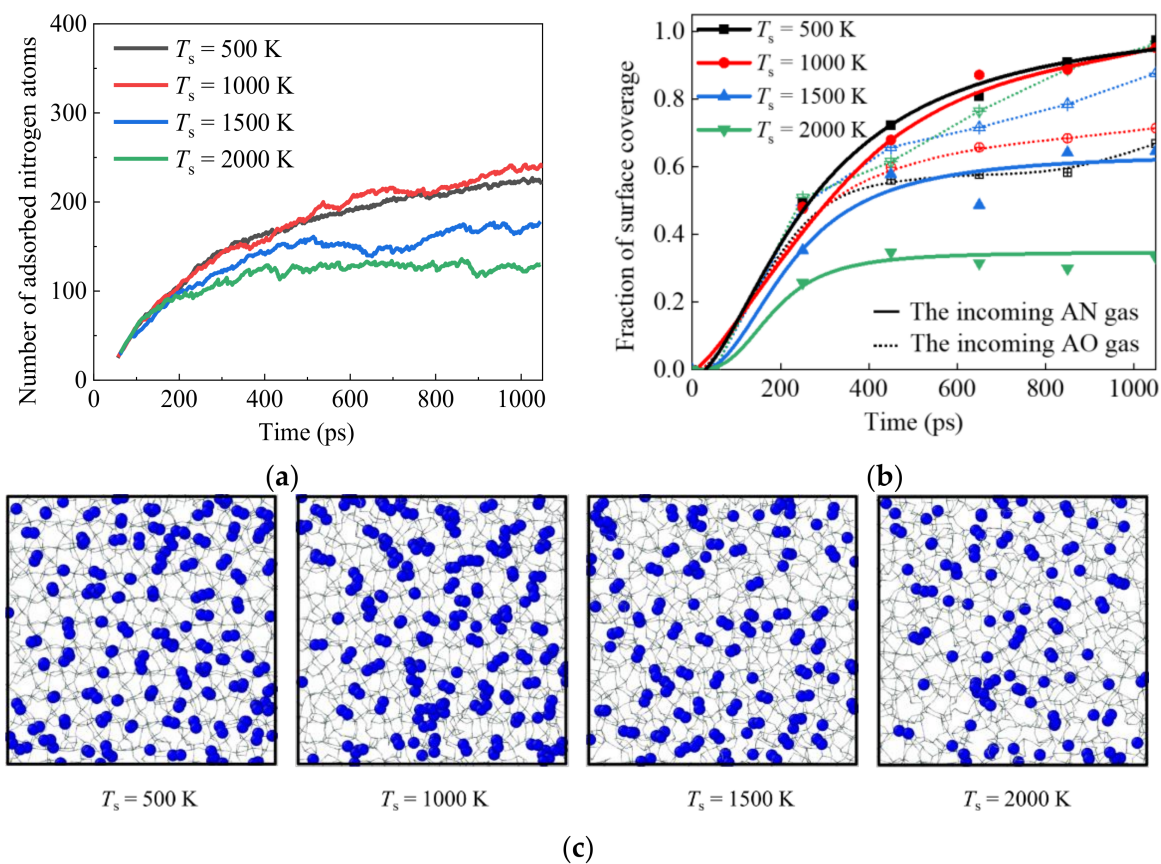


**Figure 11.** Adsorption of nitrogen atoms on the silica surface with variations in time for the case with the incoming AN gas (Models IV-17–20): (a) the effect of surface temperature on the surface adsorption, (b) the effect of surface temperature on the surface coverage fraction, and (c) snapshots for the final AN surface adsorption status from the view of the x–y plane.

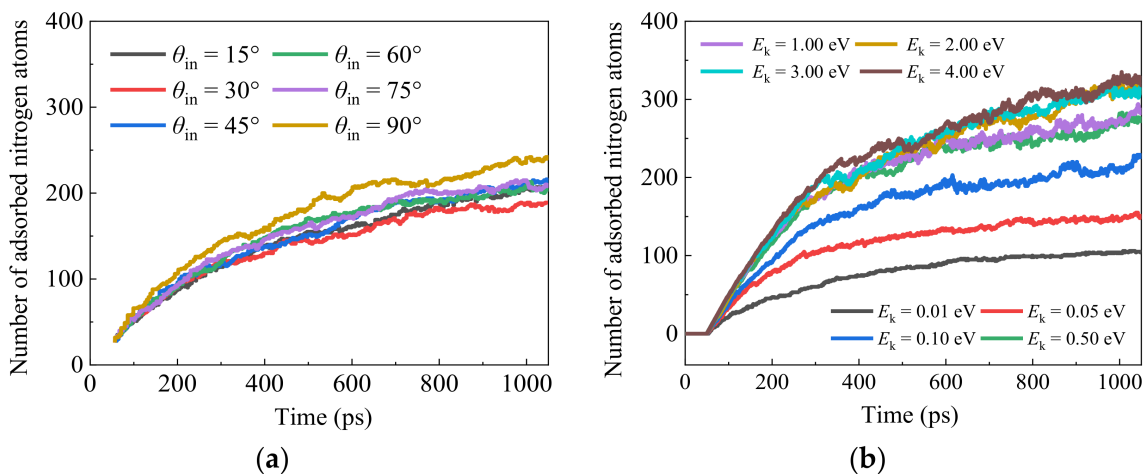


**Figure 12.** Adsorption of nitrogen atoms on the silica surface with variations in time for the case with the incoming AN gas. (a) The effect of incident angle on the surface adsorption by Models IV-21–26, and (b) the effect of incident translational energy on the surface by Models IV-27–34.

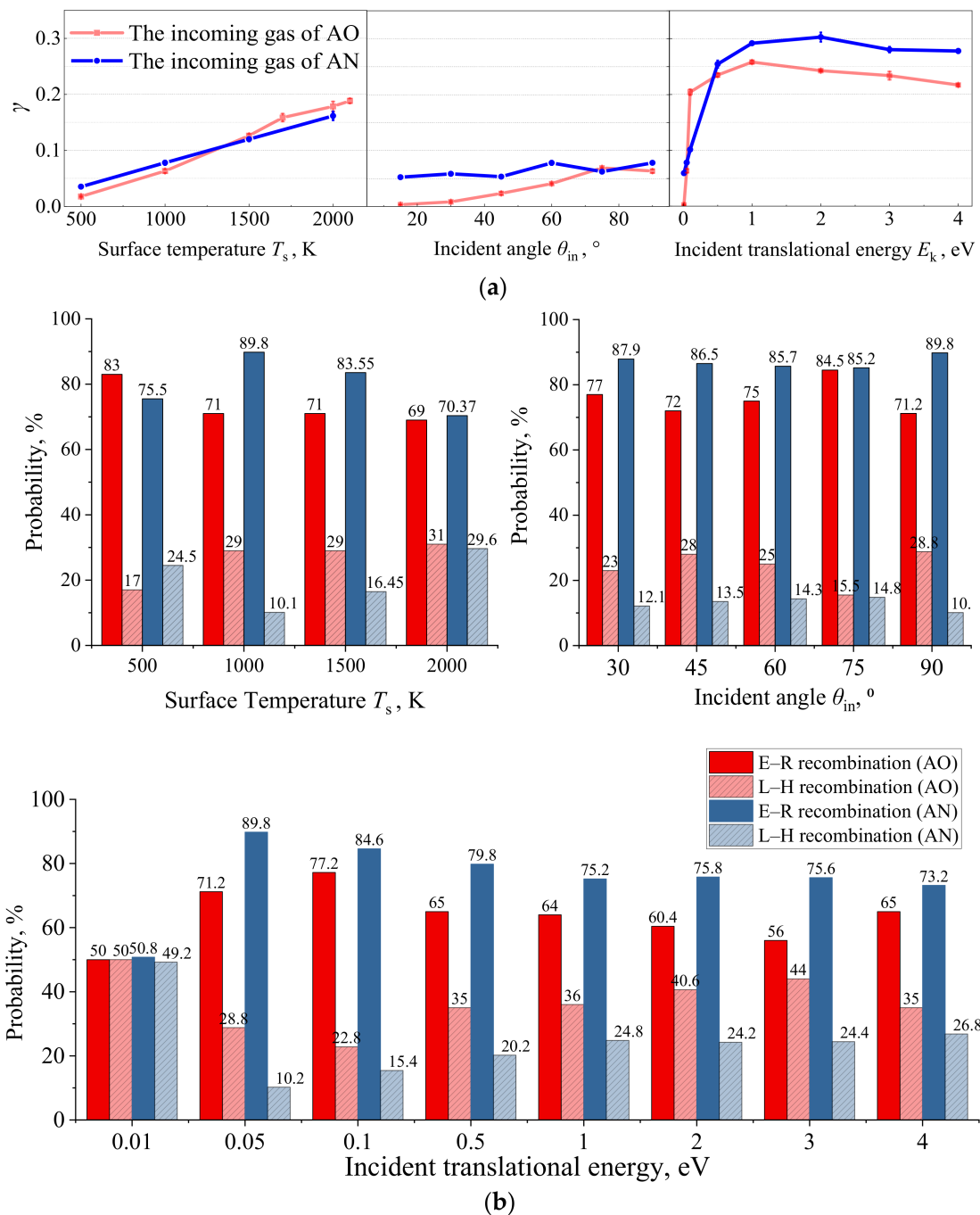


**Figure 13.** Silicon dioxide surface catalytic recombination coefficient and reaction mechanism analysis for the case with the incoming gas containing full AN (Models IV-17–34). (a) Surface catalysis recombination coefficient calculations. (b) Recombination mechanism analysis.

### 3.4. Effects of Bicomponent AO/AN Gas Mixture

To further identify the multicomponent gas effect on the surface catalysis recombination characteristics, a gaseous mixture containing both oxygen and nitrogen atoms is considered as the incidence gas with four various quantitative proportions  $f_{O/mixture} = 75\%$ , 50%, 25%, and 0% (full atomic nitrogen incidence), and compared with the standard benchmarking model that contains 100% AO as the incoming gas.

The gaseous generation components during the continuous bombardment at the gas–solid interface for silica surface are analyzed as shown in Figure 14. It can be noticed from the main reaction products for the AN/AO mixture impingement that only a few nitric

oxide molecules are found among all the gas-phase products. The gaseous productions for all the models are dominated by the molecular oxygen and nitrogen as the typical silica surface catalysis recombination reactions. Little NO and other species are found in the gaseous productions. No silicon-containing substance is found in the gaseous products, which means the silica surface plays the role of catalyzer during the recombination reactions. Compared with the gas column model established by Cozmuta et al. [54], the flux boundary conditions employed in this work significantly reduce the generation of unstable reaction products such as  $O_3N$ ,  $ON_3$ ,  $ON_4$ ,  $ON_5$ , and  $O_2N_3$  found from the results of Cozmuta et al. [54], indicating the effectiveness and benefits of the flux boundary applied in the work compared with the original gas column model.

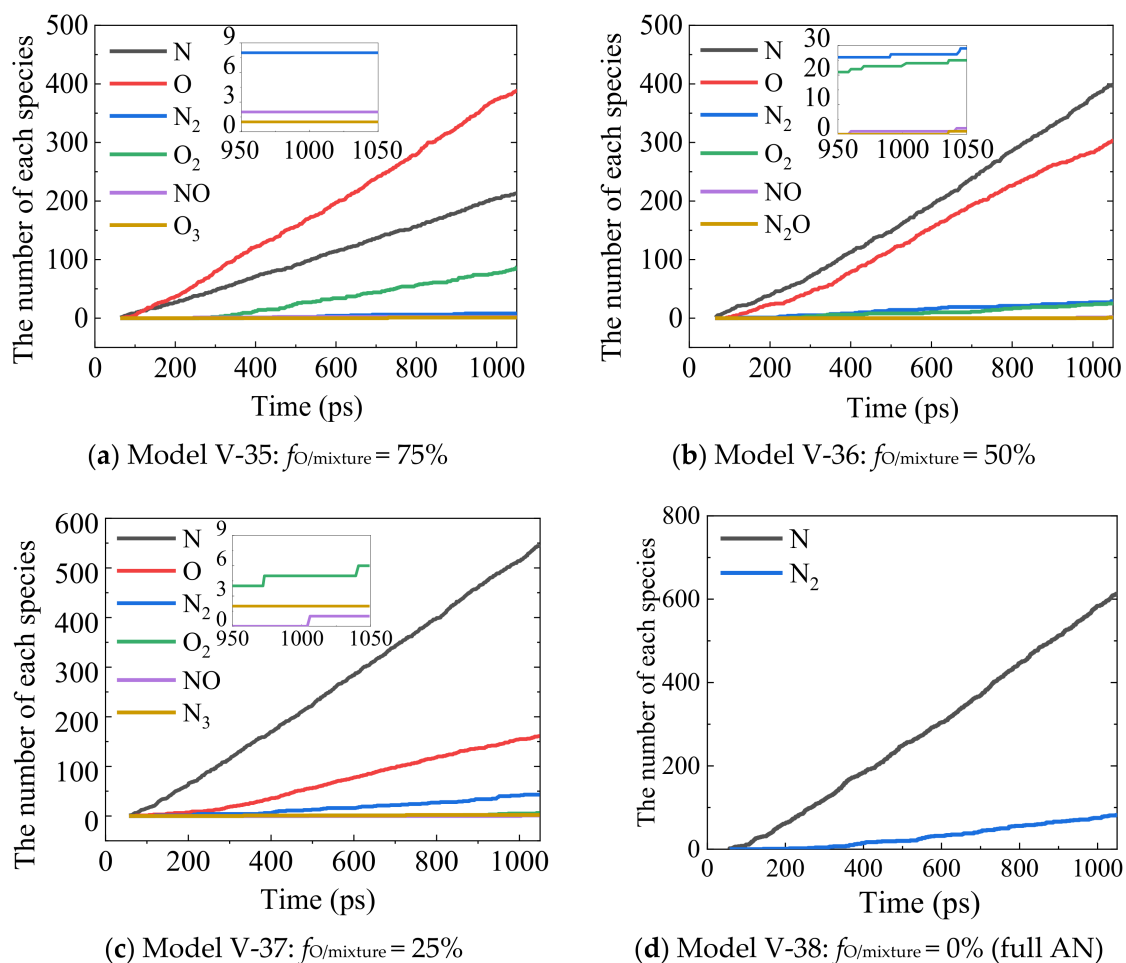


**Figure 14.** Surface catalytic reaction products. (a) Model V-35:  $f_{O/mixture} = 75\%$ , (b) Model V-36:  $f_{O/mixture} = 50\%$ , (c) Model V-37:  $f_{O/mixture} = 25\%$ , and (d) Model V-38:  $f_{O/mixture} = 0\%$  (full nitrogen).

To quantify the surface catalysis recombination coefficients of both oxygen and nitrogen for the bicomponent gas mixture bombardment, the transient surface adsorption properties and surface recombination coefficients are presented as shown in Figure 15, associated with the final surface saturation snapshots for each model. It can be found that the corresponding surface catalysis coefficient is not the simple superposition of the incoming gas mixtures: (I) with the decrease in the proportion of O atoms in the high enthalpy gas flow from  $f_{O/mixture} = 75\%$  to  $0\%$ , both the number of oxygen atoms adsorbed on the surface and the oxygen catalytic recombination coefficient (0.083, 0.025, 0.006 and 0.0) are decreased, corresponding to an increase in the number of ANs attached to the surface and the nitrogen catalytic recombination coefficient (i.e., 0.009, 0.029, 0.044 and 0.060). (II) When the proportion of O and N atoms in the impinging high enthalpy atomic flow is equal (50%), the number of O atoms adsorbed on the surface is found higher than that of N atoms. This can

be explained by Si–O chemical bond energy ( $\sim 452$  kJ/mol) being higher than Si–N chemical bond energy ( $\sim 355$  kJ/mol) [54]. However, the recombination coefficient  $\gamma_{O_2}$  is lower than  $\gamma_{N_2}$  due to their intramolecular bond energy differences. (III) For  $f_{O/mixture} = 75\%$ , the AO adsorption rate on the silica surface and the surface recombination coefficient is slightly higher than that of pure AO impinging flow ( $f_{O/mixture} = 100\%$ ). This can be explained by the potential reason of denser and more even AO adsorption distribution (intermolecular energy) onto the silica surface under the effect of extra atomistic interactions due to the existence of AN.

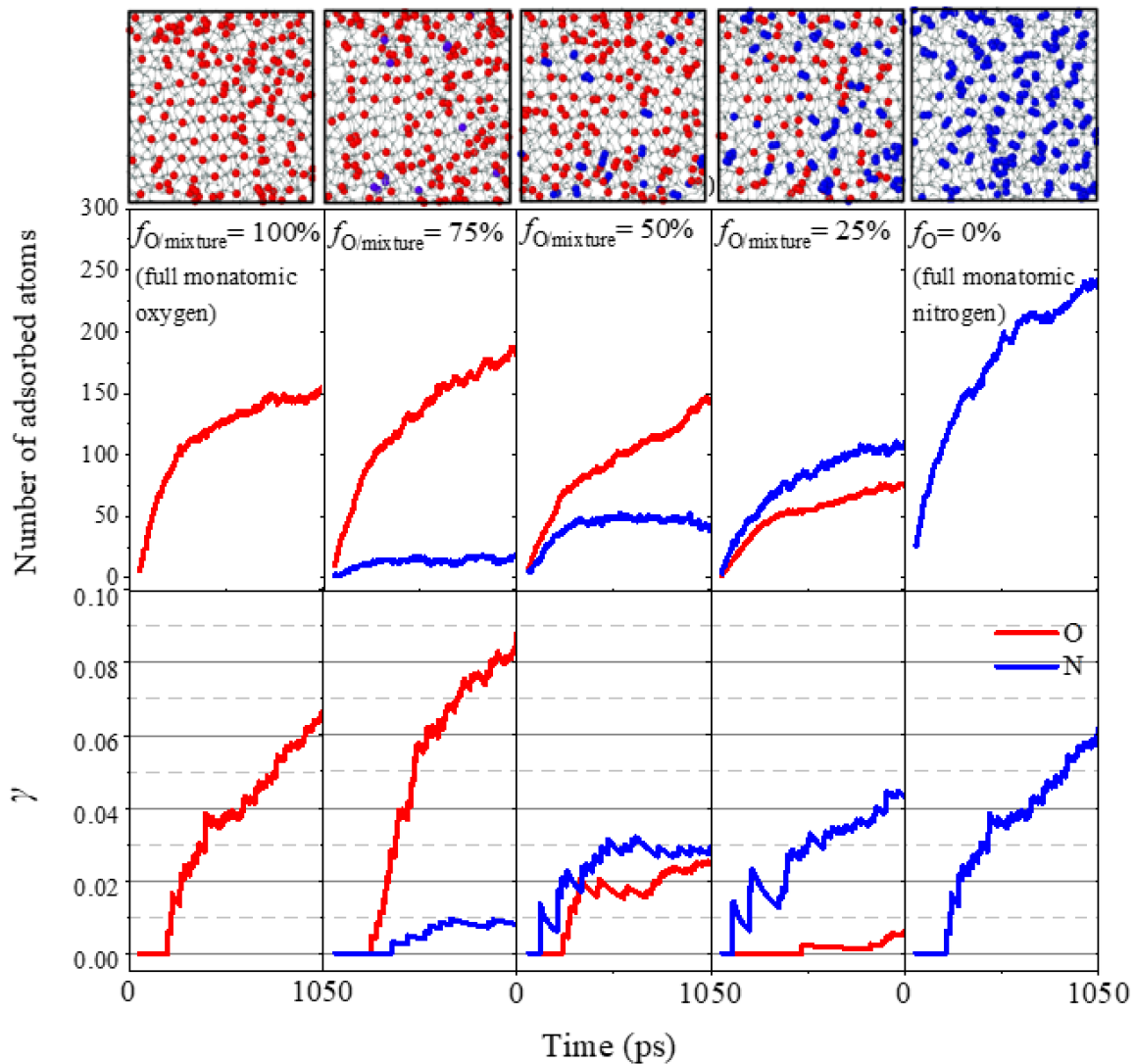


**Figure 15.** The multicomponent gas effects on the silica surface catalytic characteristics.

#### 4. Conclusions

In this study, a GSI model with a flux boundary was established to investigate the surface catalysis recombination mechanisms for silica surfaces under hyperthermal flows. Using the RMD simulation method, the effects of solid surface temperature, gas incident angle, and translational energy on the silica surface catalysis recombination were qualified in the presence of AO, AN, and various AN/AO mixtures. The main conclusions can be drawn as follows:

1. With the increase in the silica surface temperature  $T_s$  from 500 K to 2000 K, the surface coverage fraction of AO becomes greater due to the increased number of active sites on the silica surface, which enhances the percentages of L–H recombination reactions with diffusion recombination mechanisms for molecular oxygen formation.

2. The catalysis recombination coefficient  $\gamma$  under hyperthermal AO impacts is sensitive to the solid surface temperature, the gas angles of attack, and the incidence translational energy. A non-linear increasing pattern of  $\gamma_{\text{O}_2}$  with the increase in AO incident angle  $\theta_{\text{in}}$  and translational energy  $E_k$  is observed. There is an optimal relationship between the incident angle and translational energy to achieve the highest surface catalytic recombination rate. High vertical-component kinetic energy may lead AO to directly bounce away from the surface without participating in the surface catalysis recombination reactions.
3. Compared with the surface catalysis under hyperthermal AO impact, the AN surface adsorption fraction shows an inverse trend with the increase in surface temperature, which suggests the potential inadequacy of the traditional proportional-relationship assumption between the surface adsorption concentration and the surface catalysis recombination coefficient for other species, except the AO.
4. For bi-component AO/AN gas mixtures, the corresponding surface catalysis coefficient is not the simple superposition of the effects of individual gases but is affected by both the intramolecular bond energies of  $\text{O}_2$  and  $\text{N}_2$  and intermolecular energies (e.g., Si/N, Si/O), potentially varying the surface adsorption fraction and distribution.

**Author Contributions:** Conceptualization, J.Z. and D.W.; Data curation, L.H.; Formal analysis, L.H. and X.S.; Funding acquisition, J.Z. and D.W.; Investigation, L.H. and Z.C.; Methodology, Z.C. and X.S.; Project administration, J.Z. and D.W.; Supervision, J.Z. and D.W.; Validation, Z.C.; Visualization, L.H., Z.C. and X.S.; Writing—original draft, L.H.; Writing—review & editing, J.Z. and D.W. All authors have read and agreed to the published version of the manuscript.

**Funding:** Manned Space Engineering Technology (No. ZS2020103001); The National Natural Science Foundation of China (No. 52006004); The National Natural Science Foundation of China-Deutsche Forschungsgemeinschaft Mobility Programme (No. M-0368).

**Institutional Review Board Statement:** Not applicable.

**Informed Consent Statement:** Not applicable.

**Data Availability Statement:** Data available on request.

**Conflicts of Interest:** The authors declare no conflict of interest.

## References

1. Weidner, J.P. Hypersonic propulsion—Breaking the thermal barrier. *Proc. Inst. Mech. Eng. Part G J. Aerosp. Eng.* **1993**, *207*, 47–59. [[CrossRef](#)]
2. Chen, Y.; Zhang, R.; Zhang, G.; Jiang, P.; Song, J.; Chu, X. Toughening mechanism of thermal barrier coatings. *Int. J. Thermophys.* **2021**, *42*, 69. [[CrossRef](#)]
3. Zhong, X. High-order finite-difference schemes for numerical simulation of hypersonic boundary-layer transition. *J. Comput. Phys.* **1998**, *144*, 662–709. [[CrossRef](#)]
4. Takahashi, Y.; Yamada, K. Aerodynamic heating of inflatable aeroshell in orbital reentry. *Acta Astronaut.* **2018**, *152*, 437–448. [[CrossRef](#)]
5. Mankodi, T.K.; Myong, R. Quasi-classical trajectory-based non-equilibrium chemical reaction models for hypersonic air flows. *Phys. Fluids A* **2019**, *31*, 106102. [[CrossRef](#)]
6. Borrelli, R.; Riccio, A.; Tescione, D.; Gardi, R.; Marino, G. Thermo-structural behaviour of an UHTC made nose cap of a reentry vehicle. *Acta Astronaut.* **2009**, *65*, 442–456. [[CrossRef](#)]
7. Maus, J.; Griffith, B.; Szema, K.; Best, J. Hypersonic Mach number and real gas effects on Space Shuttle Orbiteraerodynamics. *J. Spacecr. Rocket.* **1984**, *21*, 136–141. [[CrossRef](#)]
8. Satheesh Chandran, M.; Sunitha, K.; Uday Bhaskar, N.; Santhosh Kumar, K.; Sreenivas, N.; Mathew, D. Low Density Syntactic Foam Composites as Ablative TPS Material for High Heat Flux Conditions for Reentry Missions. *Trans. Indian Natl. Acad. Eng.* **2021**, *6*, 153–158. [[CrossRef](#)]
9. Barbato, M.; Giordano, D.; Muylaert, J.; Bruno, C.R. Comparison of catalytic wall conditions for hypersonic flow. *J. Spacecr.* **1996**, *33*, 620–627. [[CrossRef](#)]
10. Behrens, B.; Mueller, M. Technologies for thermal protection systems applied on re-usable launcher. *Acta Astronaut.* **2004**, *55*, 529–536. [[CrossRef](#)]
11. Yi, J.; He, X.; Sun, Y.; Li, Y. Electron beam-physical vapor deposition of SiC/SiO<sub>2</sub> high emissivity thin film. *Appl. Surf. Sci.* **2007**, *253*, 4361–4366. [[CrossRef](#)]



12. Kim, I.; Lee, S.; Kim, J.G.; Park, G. Analysis of nitrogen recombination activity on silicon dioxide with stagnation heat-transfer. *Acta Astronaut.* **2020**, *177*, 386–397. [[CrossRef](#)]
13. Paterna, D.; Monti, R.; Savino, R.; Esposito, A. Experimental and numerical investigation of Martian atmosphere entry. *J. Spacecr. Rocket.* **2002**, *39*, 227–236. [[CrossRef](#)]
14. Serpico, M.; Monti, R.; Savino, R. Heat flux on partially catalytic surfaces in hypersonic flows. *J. Spacecr. Rocket.* **1998**, *35*, 9–15. [[CrossRef](#)]
15. Armenise, I.; Barbato, M.; Capitelli, M.; Kustova, E.; Transfer, H. State-to-State Catalytic Models, Kinetics, and Transport in Hypersonic Boundary Layers. *J. Thermophys. Heat Transf.* **2006**, *20*, 465–476. [[CrossRef](#)]
16. Nasuti, F.; Barbato, M.; Bruno, C. Material-dependent catalytic recombination modeling for hypersonic flows. *J. Thermophys. Heat Transf.* **1996**, *10*, 131–136. [[CrossRef](#)]
17. Herdrich, G.; Auweter-Kurtz, M.; Lhle, S.; Pidan, S.; Laux, T. Oxidation Behavior of SiC-based Thermal Protection System Materials Using Newly Developed Probe Techniques. In Proceedings of the 37th AIAA Thermophysics Conference, Portland, OR, USA, 28 June–1 July 2004.
18. Park, C.; Jaffe, R.L.; Partridge, H. Chemical-kinetic parameters of hyperbolic earth entry. *J. Thermophys. Heat Transf.* **2001**, *15*, 76–90. [[CrossRef](#)]
19. Li, K.; Liu, J.; Liu, W. A new surface catalytic model for silica-based thermal protection material for hypersonic vehicles. *Chin. J. Aeronaut.* **2015**, *28*, 1355–1361. [[CrossRef](#)]
20. Yang, X.; Gui, Y.; Tang, W.; Du, Y.; Wei, D.; Xiao, G.; Liu, L. Surface chemical effects on hypersonic nonequilibrium aeroheating in dissociated carbon–oxygen mixture. *J. Spacecr. Rocket.* **2018**, *55*, 687–697. [[CrossRef](#)]
21. Scott, C. Catalytic recombination of nitrogen and oxygen on iron-cobalt-chromia spinel. In Proceedings of the 21st Aerospace Sciences Meeting, Reno, NV, USA, 10–13 January 1983.
22. Carandente, V.; Savino, R.; Esposito, A.; Zuppari, G.; Caso, V. Experimental and numerical simulation, by an arc-jet facility, of hypersonic flow in Titan’s atmosphere. *Exp. Therm. Fluid Sci.* **2013**, *48*, 97–101. [[CrossRef](#)]
23. Balat-Pichelin, M.; Badie, J.M.; Berjoan, R.; Boubert, P. Recombination coefficient of atomic oxygen on ceramic materials under earth re-entry conditions by optical emission spectroscopy. *Chem. Phys.* **2003**, *291*, 181–194. [[CrossRef](#)]
24. Dickens, P.G.; Sutcliffe, M.B. Recombination of oxygen atoms on oxide surfaces. Part 1—Activation energies of recombination. *Trans. Faraday Soc.* **1964**, *60*, 1272–1285. [[CrossRef](#)]
25. Stewart, D. Determination of surface catalytic efficiency for thermal protection materials—Room temperature to their upper use limit. In Proceedings of the 31st Thermophysics Conference, New Orleans, LA, USA, 18–20 June 1996.
26. Kim, Y.C.; Boudart, M. Recombination of oxygen, nitrogen, and hydrogen atoms on silica: Kinetics and mechanism. *Langmuir* **1991**, *7*, 2999–3005. [[CrossRef](#)]
27. Carleton, K.L.; Marinelli, W.J. Spacecraft thermal energy accommodation from atomic recombination. *J. Thermophys. Heat Transf.* **1992**, *6*, 650–655. [[CrossRef](#)]
28. Rutigliano, M.; Cacciatore, M. Recombination of Oxygen Atoms on Silica Surface: New and More Accurate Results. *J. Thermophys. Heat Transf.* **2015**, *30*, 247–250. [[CrossRef](#)]
29. Miller, J.H.; Tennehill, J.C.; Wadawadigi, G.; Edwards, T.A.; Lawrence, S.L. Computation of hypersonic flows with finite catalytic walls. *J. Thermophys. Heat Transf.* **1995**, *9*, 486–493. [[CrossRef](#)]
30. Nguyen, V.T.; Fang, T.H. Material removal and wear mechanism in abrasive polishing of SiO<sub>2</sub>/SiC using molecular dynamics. *Ceram. Int.* **2020**, *46*, 21578–21595. [[CrossRef](#)]
31. Chen, J.; Shi, J.; Chen, Z.; Zhang, M.; Peng, W.; Fang, L.; Sun, K.; Han, J. Mechanical properties and deformation behaviors of surface-modified silicon: A molecular dynamics study. *J. Mater. Sci.* **2019**, *54*, 3096–3110. [[CrossRef](#)]
32. Li, W.; Garofalini, S.H. Molecular dynamics simulation of lithium diffusion in Li<sub>2</sub>O–Al<sub>2</sub>O<sub>3</sub>–SiO<sub>2</sub> glasses. *Solid State Ion.* **2004**, *166*, 365–373. [[CrossRef](#)]
33. Van Duin, A.C.; Dasgupta, S.; Lorant, F.; Goddard, W.A. ReaxFF: A Reactive Force Field for Hydrocarbons. *J. Phys. Chem. A* **2001**, *105*, 9396–9409. [[CrossRef](#)]
34. Chenoweth, K.; Van Duin, A.C.; Goddard, W.A. ReaxFF Reactive Force Field for Molecular Dynamics Simulations of Hydrocarbon Oxidation. *J. Phys. Chem. A* **2008**, *112*, 1040–1053. [[CrossRef](#)]
35. Raymand, D.; van Duin, A.C.; Baudin, M.; Hermansson, K. A reactive force field (ReaxFF) for zinc oxide. *Surf. Sci.* **2008**, *602*, 1020–1031. [[CrossRef](#)]
36. Wang, N.; Feng, Y.; Guo, X. Atomistic mechanisms study of the carbonation reaction of CaO for high-temperature CO<sub>2</sub> capture. *Appl. Surf. Sci.* **2020**, *532*, 147425. [[CrossRef](#)]
37. Feng, M.; Jiang, X.Z.; Luo, K.H. A reactive molecular dynamics simulation study of methane oxidation assisted by platinum/graphene-based catalysts. *Proc. Combust. Inst.* **2019**, *37*, 5473–5480. [[CrossRef](#)]
38. Hasan, R.M.M.; Politano, O.; Luo, X. ReaxFF molecular dynamics simulation study of nanoelectrode lithography oxidation process on silicon (100) surface. *Appl. Surf. Sci.* **2019**, *496*, 143679. [[CrossRef](#)]
39. Cui, Z.; Yao, G.; Zhao, J.; Zhang, J.; Wen, D. Atomistic-scale investigations of hyperthermal oxygen–graphene interactions via reactive molecular dynamics simulation: The gas effect. *Phys. Fluids* **2021**, *33*, 052107. [[CrossRef](#)]
40. Cui, Z.; Zhao, J.; He, L.; Jin, H.; Zhang, J.; Wen, D. A reactive molecular dynamics study of hyperthermal atomic oxygen erosion mechanisms for graphene sheets. *Phys. Fluids* **2020**, *32*, 112110. [[CrossRef](#)]

41. Bačová, P.; Li, W.; Behbahani, A.F.; Burkhart, C.; Polińska, P.; Doxastakis, M.; Harmandaris, V. Coupling between Polymer Conformations and Dynamics Near Amorphous Silica Surfaces: A Direct Insight from Atomistic Simulations. *Nanomaterials* **2021**, *11*, 2075. [[CrossRef](#)]
42. Gai, L.; Shin, Y.K.; Raju, M.; Van Duin, A.C.T.; Raman, S. Atomistic Adsorption of Oxygen and Hydrogen on Platinum Catalysts by Hybrid Grand Canonical Monte Carlo/Reactive Molecular Dynamics. *J. Phys. Chem. C* **2016**, *120*, 9780–9793. [[CrossRef](#)]
43. Jeon, B.; Sankaranarayanan, S.K.R.S.; Van Duin, A.C.T.; Ramanathan, S. Influence of surface orientation and defects on early-stage oxidation and ultrathin oxide growth on pure copper. *Philos. Mag.* **2011**, *91*, 4073–4088. [[CrossRef](#)]
44. Valentini, P.; Schwartzentruber, T.E.; Cozmuta, I. Molecular dynamics simulation of O<sub>2</sub> sticking on Pt(111) using the ab initio based ReaxFF reactive force field. *J. Chem. Phys.* **2010**, *133*, 084703. [[CrossRef](#)] [[PubMed](#)]
45. Sun, Y.; Liu, Y.; Chen, X.; Zhai, Z.; Xu, F.; Liu, Y. Micromechanism of oxygen transport during initial stage oxidation in Si(100) surface: A ReaxFF molecular dynamics simulation study. *Appl. Surf. Sci.* **2017**, *406*, 178–185. [[CrossRef](#)]
46. Cao, H.; Pamungkas, M.A.; Kim, B.H.; Lee, K.R. A Molecular Dynamics Simulation Study on the Initial Stage of Si(001) Oxidation Under Biaxial Strain. *J. Nanosci. Nanotechnol.* **2013**, *13*, 1074–1077. [[CrossRef](#)] [[PubMed](#)]
47. Newsome, D.A.; Sengupta, D.; Foroutan, H.; Russo, M.F.; Van Duin, A.C.T. Oxidation of Silicon Carbide by O<sub>2</sub> and H<sub>2</sub>O: A ReaxFF Reactive Molecular Dynamics Study, Part I. *J. Phys. Chem. C* **2012**, *116*, 16111–16121. [[CrossRef](#)]
48. Gamallo, P.; Prats, H.; Sayos, R. ReaxFF molecular dynamics simulations of CO collisions on an O-preadsorbed silica surface. *J. Mol. Model.* **2014**, *20*, 2160. [[CrossRef](#)]
49. Mao, Q.; Van Duin, A.C.T.; Luo, K.H. Investigation of methane oxidation by palladium-based catalyst via ReaxFF Molecular Dynamics simulation. *Proc. Combust. Inst.* **2017**, *36*, 4339–4346. [[CrossRef](#)]
50. Khalilov, U.; Pourtois, G.; Van Duin, A.C.T.; Neyts, E.C. Hyperthermal Oxidation of Si(100)2x1 Surfaces: Effect of Growth Temperature. *J. Phys. Chem. C* **2012**, *116*, 8649–8656. [[CrossRef](#)]
51. Khalilov, U.; Pourtois, G.; Huygh, S.; Van Duin, A.C.T.; Neyts, E.C.; Bogaerts, A. New Mechanism for Oxidation of Native Silicon Oxide. *J. Phys. Chem. C* **2013**, *117*, 9819–9825. [[CrossRef](#)]
52. Khalilov, U.; Neyts, E.C.; Pourtois, G.; Van Duin, A.C.T. Can We Control the Thickness of Ultrathin Silica Layers by Hyperthermal Silicon Oxidation at Room Temperature? *J. Phys. Chem. C* **2011**, *115*, 24839–24848. [[CrossRef](#)]
53. Yang, Y.; Peddakotla, S.A.; Kumar, R.; Park, G. Microscopic Analysis of Catalytic Recombination Process. In Proceedings of the 2019 World Congress on Advances in Nano, Bio, Robotics and Energy (ANBRE19), Jeju Island, Korea, 17–21 September 2019.
54. Cozmuta, I. Molecular mechanisms of gas surface interactions in hypersonic flow. In Proceedings of the 39th AIAA Thermophysics Conference, Miami, FL, USA, 25–28 June 2007.
55. Norman, P.E. Modeling Air-Silica Surface Catalysis in Hypersonic Environments Using ReaxFF Molecular Dynamics. Master's Thesis, University of Minnesota, Minneapolis, MN, USA, May 2010.
56. Norman, P.; Schwartzentruber, T.; Cozmuta, I. Modeling Air-SiO<sub>2</sub> Surface Catalysis under Hypersonic Conditions with ReaxFF Molecular Dynamics. In Proceedings of the 10th AIAA/ASME Joint Thermophysics and Heat Transfer Conference, Chicago, IL, USA, 28 June–1 July 2010.
57. Norman, P.; Schwartzentruber, T.E.; Leverentz, H.; Luo, S.; Meana-Pañeda, R.; Paukku, Y.; Truhlar, D.G. The structure of silica surfaces exposed to atomic oxygen. *J. Phys. Chem. C* **2013**, *117*, 9311–9321. [[CrossRef](#)]
58. Norman, P.; Schwartzentruber, T. A Finite-Rate Model for Oxygen-Silica Catalysis through Computational Chemistry Simulation. In Proceedings of the 28th International Symposium on Rarefied Gas Dynamics, Zaragoza, Spain, 9–13 July 2012.
59. Cui, Z.; Jin, Z.; Yao, G.; Jun, Z.; Li, Z.; Tang, Z.; Wen, D. Competing effects of surface catalysis and ablation in hypersonic reentry aerothermodynamic environment. *Chin. J. Aeronaut.* **2021**, *in press*. [[CrossRef](#)]
60. Plimpton, S.; Crozier, P.; Thompson, A. LAMMPS-large-scale atomic/molecular massively parallel simulator. *Sandia Natl. Lab.* **2007**, *18*, 43.
61. Kulkarni, A.D.; Truhlar, D.G.; Goverapet Srinivasan, S.; Van Duin, A.C.; Norman, P.; Schwartzentruber, T.E. Oxygen interactions with silica surfaces: Coupled cluster and density functional investigation and the development of a new ReaxFF potential. *J. Phys. Chem. C* **2013**, *117*, 258–269. [[CrossRef](#)]
62. Pastor, R.W.; Brooks, B.R.; Szabo, A. An analysis of the accuracy of Langevin and molecular dynamics algorithms. *Mol. Phys.* **1988**, *65*, 1409–1419. [[CrossRef](#)]
63. Deutschmann, O.; Riedel, U.; Warnatz, J. Modeling of nitrogen and oxygen recombination on partial catalytic surfaces. *J. Heat Transf.* **1995**, *117*, 495–501. [[CrossRef](#)]